A New Approach to Determining Gas-Particle Reaction Probabilities and Application to the Heterogeneous Reaction of Deliquesced Sodium Chloride Particles with Gas-Phase Hydroxyl Radicals

Alexander Laskin,*,† Hai Wang,‡ William H. Robertson,§ James P. Cowin,|| Michael J. Ezell,§ and Barbara J. Finlayson-Pitts§

W. R. Wiley Environmental Molecular Science Laboratory, Pacific Northwest National Laboratory, Richland, Washington 99352, Department of Aerospace and Mechanical Engineering, University of Southern California, Los Angeles, California 90089-1453, Department of Chemistry, University of California, Irvine, Irvine, California 92697-2025, and Chemical Sciences Division, Pacific Northwest National Laboratory, Richland, Washington 99352

Received: May 26, 2006; In Final Form: July 14, 2006

The reaction kinetics for gaseous hydroxyl radicals (OH) with deliquesced sodium chloride particles ($NaCl_{aq}$) were investigated using a novel experimental approach. The technique utilizes the exposure of substrate-deposited aerosol particles to reactive gases followed by chemical analysis of the particles using computer-controlled scanning electron microscopy with energy-dispersive analysis of X-rays (CCSEM/EDX) capability. Experiments were performed at room temperature and atmospheric pressure with deliquesced NaCl particles in the micron size range at 70−80% RH and with OH concentrations in the range of 1 to 7×10^9 cm^{-3}. The apparent, pseudo first-order rate constant for the reaction was determined from measurements of changes in the chloride concentration of individual particles upon reaction with OH as a function of the particle loading on the substrate. Quantitative treatment of the data using a model that incorporates both diffusion and reaction kinetics yields a lower limit to the net reaction probability of $\gamma_{net} \geq 0.1$, with an overall uncertainty of a factor of 2.

Introduction

An understanding of the uptake and reaction kinetics of gases into aqueous sea salt particles is of key importance to elucidating atmospheric chemical processes in areas influenced by marine aerosol. It has been recognized for at least 50 years that sea salt particles react in air with trace gases such as NO_2, HNO_3, H_2SO_4, O_3, OH, N_2O_5, and $ClONO_2$ to convert the halide ions into various gas-phase halogen products.[1−47] Some of these products,[40,41,46] such as ClNO, $ClNO_2$, and Cl_2, photodissociate into highly reactive chlorine atoms (Cl) under sunlight (>290 nm). Once formed, Cl reacts predominantly with organics, leading to ozone formation,[48] and in this way, it can contribute significantly to the chemistry of the marine boundary layer and coastal areas.

Sea salt aerosol is generated by wave action and bursting of bubbles over marine surfaces.[49−52] As droplets of sea salt aerosol are transported inland, some water can evaporate, leaving behind either concentrated aqueous droplets of deliquesced sea salt or, at sufficiently low relative humidity (RH), particles with a crystalline core. At the ambient temperature of 298 K, the deliquescence and efflorescence RHs of pure NaCl are ∼75% and ∼44%, respectively.[53] Sea salt is a mixture of salts, including some that are highly soluble and hygroscopic, e.g., $MgCl_2 \cdot 6H_2O$, $KMgCl_3 \cdot 6H_2O$, and $MgSO_4 \cdot H_2O$.[54] These salts remain deliquesced and form a liquid coating around the NaCl crystalline core at RHs as low as 10−20% RH.[55] Under typical tropospheric conditions, the relative humidity is generally high enough so that sea salt particles are either fully or partially deliquesced.

A number of recent laboratory and modeling studies indicate that aqueous sea salt particles may serve as an important source of gaseous molecular chlorine and bromine due to unique chemistry that occurs at the air−water interface.[56−72] For example, a combination of aerosol chamber experiments, kinetic modeling, and molecular dynamic simulations has led to the conclusion that the underlying mechanism of Cl_2 production from the reaction of deliquesced NaCl particles with hydroxyl (OH) radicals is driven by interface chemistry.[67] More specifically, as gas-phase OH radicals are scavenged at the particle surface, surface complexes $(OH\cdots Cl^-)_{surface}$ are formed

$$OH_g + Cl^-_{surface} \rightarrow (OH\cdots Cl^-)_{surface} \qquad \text{(R1)}$$

These surface complexes react further in an as yet unknown reaction sequence that yields molecular chlorine, Cl_2. Possibilities include, for example, self-reaction of the surface complexes (R2)

$$(OH\cdots Cl^-)_{surface} + (OH\cdots Cl^-)_{surface} \rightarrow Cl_{2g} + 2OH^-_{aq} \qquad \text{(R2)}$$

or reaction of the complex with Cl^- followed by secondary chemistry.[67,73] In any event, the net reaction is given by reaction (R3)

$$Cl^-_{surface} + OH_g \rightarrow {}^1/_2 Cl_{2,g} + OH^-_{aq} \qquad \text{(R3)}$$

* Corresponding author. E-mail: Alexander.Laskin@pnl.gov.
† W. R. Wiley Environmental Molecular Science Laboratory, Pacific Northwest National Laboratory.
‡ University of Southern California.
§ University of California.
|| Chemical Sciences Division, Pacific Northwest National Laboratory.

10.1021/jp063263+ CCC: $33.50
Published on Web 08/23/2006

There are as yet no direct experimental measurements of the kinetics of this reaction. While a net reaction probability of $\gamma = 0.2$ was used to match the experimental data in the modeling studies of Knipping and Dabdub,[73] there were a number of variables in the model so that the net reaction probability was not uniquely defined by the data.

Here, we report a relatively straightforward approach to measure a lower limit for the overall reaction probability for $NaCl_{aq} + OH_g$. This approach utilizes the exposure of substrate-deposited, deliquesced NaCl aerosol droplets to gas-phase OH followed by chemical analysis of individual particles with electron microprobe techniques.[68,74−76] As discussed below, fundamental reaction kinetics data may be obtained from these experiments after a theoretical kinetics−diffusion analysis of gaseous reactant transport from the bulk gas to the substrate surface. Such effects arise from the close proximity of the reacting particles mounted on the substrate at high particle loadings, which alter the effective gas-phase OH concentrations at the particle surface and hence the kinetics of chloride ion loss.

Experimental Methods

Materials and Sample Preparation. Monodisperse NaCl particles were generated from an aqueous 0.5 M solution of NaCl (Aldrich, Inc., 99.99% purity) using a nebulizer (TSI, Inc., model 3076). The particles were dried in a diffusion drier (TSI, Inc., model 3062) prior to sizing using a differential mobility analyzer (DMA) (TSI, Inc., model 3080L). To provide a constant stream of ~1 μm diameter dry particles, the flows in the DMA were set at 2 and 0.2 SLPM for sheath and sample flows, respectively. At these flow settings, the impactor (0.071 mm orifice) at the DMA inlet effectively traps particles larger than 1.58 μm and therefore eliminates multiply charged larger particles in the outlet stream. The resulting dry particles, approximately 1 μm in diameter, were deposited on TEM grids (Carbon Type-B, 300 mesh gold grids, Ted Pella, Inc.) using a home-built, microprocessor-controlled time-resolved aerosol collector (TRAC).[77,78] The particle loading ranges from $N_s = 1 \times 10^4$ to 5×10^7 particles/cm^2 that correspond to approximate distances between neighboring particles between 100 μm and 1.5 μm, respectively. The size uniformity of deposited particles was confirmed by computer controlled scanning electron microscopy (CCSEM) analyses over ~3000 particles in several samples, with each sample being a particular grid deposited with NaCl particles. Figure 1 shows an SEM image of a typical particle sample and the companion size distribution obtained from the equivalent, two-dimensional projection areas of the particles. The size distribution is log normal with a mean diameter equal to $\bar{D}_p = 0.91$ μm, median diameter $\langle D_p \rangle = 0.84$ μm, and geometric standard deviation $\sigma = 1.36$.

Particle Exposure Apparatus. The schematic of the experimental apparatus is shown in Figure 2. In each experiment, 5 to 6 TEM grids loaded with varying numbers of NaCl particles were placed in a photolysis cell (4 cm in diameter and 10 cm in length). The TEM grids resided in shallow depressions of a glass holder out of direct illumination. The deposited particles were exposed to a continuous flow (~2 L/min) of humidified nitrogen with controlled amounts of O_2, O_3, and OH at the ambient temperature and atmospheric pressure. The gas stream passes only over the upper surface of the grids that hold the salt. The TEM grids were placed without specific order with respect to their density and were separated by a minimal distance of 1.3 cm from one to another to minimize interference.

Hydroxyl radicals were produced by photolysis of O_3 to generate $O(^1D)$ followed by its rapid reaction with water vapor.

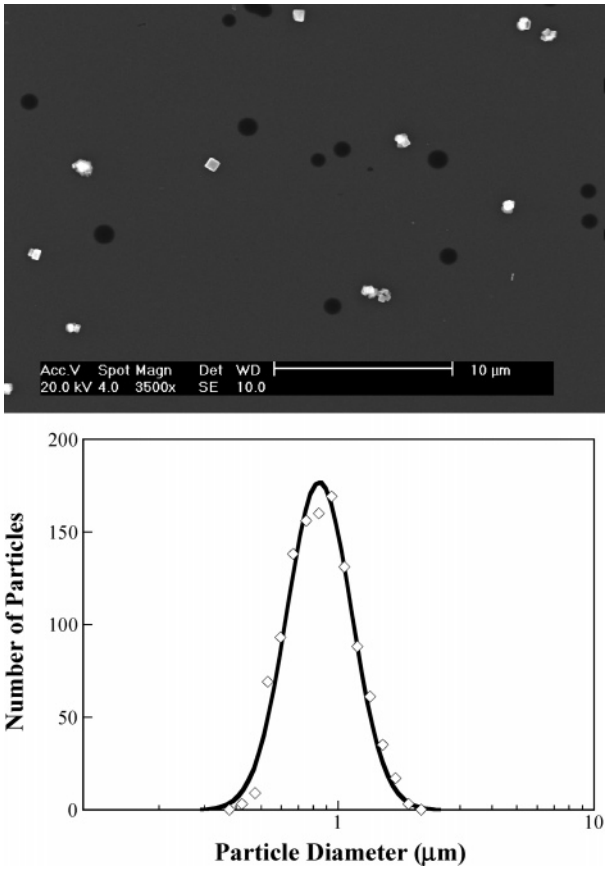

Figure 1. SEM image (top panel) and CCSEM measured particle size distribution (bottom panel) of a representative sample. The size distribution data (symbols) may be fitted by a log-normal distribution function (line) with a median diameter $\langle D_p \rangle = 0.84$ μm and geometric standard deviation $\sigma = 1.36$ (mean diameter $\bar{D}_p = 0.91$ μm). The surface density of the sample is $N_s = 1.5 \times 10^6$ cm^{-2}. Dark spots seen in the micrograph are surface features of the carbon film.

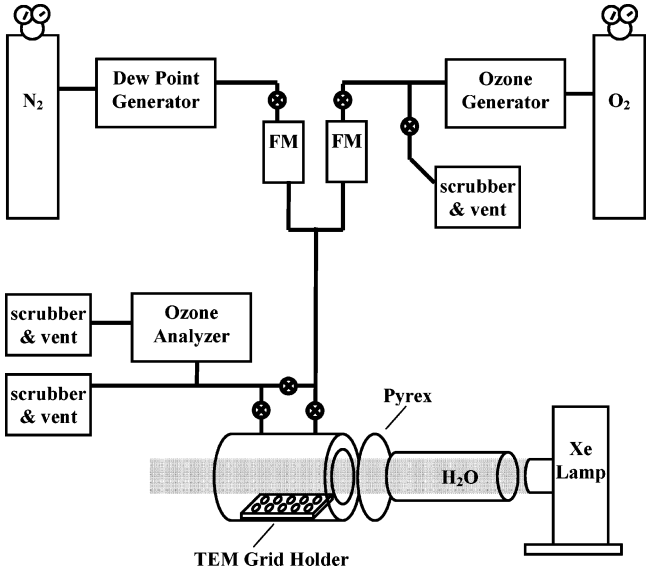

Figure 2. Schematic of flow system for reacting OH radicals with deliquesced NaCl particles sequestered on TEM grids. FM = flow meter.

A Xe arc lamp was used as the UV source (a 100 W Xe 60000 series, Oriel, Inc., or a 1000 W Xe LH-15LN/2, Schoeffel Instrument Corporation, Inc., with an LPS 255HR power supply by Kratos Analytical Instruments, Inc.). The light beam was

collimated along the length of the cell and was filtered with a 2 mm Pyrex filter ($\lambda > 300$ nm) and a 10 cm H_2O filter to suppress infrared heating of the cell. Tests were performed to measure temperature rise in the cell due to the lamp radiation using a thermocouple. The increase was found to be <1 K, which was much less than variations in the room temperature ($T = 22-26$ °C) over the course of the experiments.

The relative humidity was controlled by a dew point generator (Li-Cor, Inc., model LI-610). Ozone was generated in a small flow of dry, high-purity O_2 (≥99.993%, Airco, Inc.) through an ozone generator (Pacific Ozone Technology, Inc., model L11), which was then mixed with the humidified nitrogen flow through two independent flow meters. In this way, the O_3 and H_2O concentrations in the flow into the photolysis cell were independently varied. The ozone concentration in the photolysis cell was monitored with a photometric analyzer (Advanced Pollution Instrumentation, Inc., 450 M Ozone Monitor) connected to the outlet of the photolysis cell. The RH was periodically measured in the cell outlet using a dew point hygrometer (Vaisala, Inc., model HMP234).

The production of the OH radicals in the photolysis cell is described by the following gas-phase reactions:

$$O_3 \xrightarrow{h\nu} O(^1D) + O_2 \quad \text{(R4)}$$

$$O(^1D) + H_2O \rightarrow 2OH \quad \text{(R5)}$$

$$O(^1D) \xrightarrow{+M} O(^3P) \quad \text{(R6)}$$

$$O(^3P) + O_2 \xrightarrow{+M} O_3 \quad \text{(R7)}$$

The steady-state gas-phase OH concentrations in the free stream, i.e., unperturbed by reaction with the particles, were estimated using the *AcuChem*[79] kinetics modeling package employing reactions R4−R7 as well as the secondary chemistry of all HO_x species in the system. The rates of these reactions are well-known, so that the only variable is the ozone photolysis rate constant, k_P. The latter was determined by monitoring the decay of O_3 as a function of photolysis time in a static experiment using the same apparatus and a UV−vis spectrometer (Shimadzu, Inc., model UV-2501PC) and applying the kinetics model to determine the best-fit value of k_P. Depending on the O_3 concentration and the UV intensity, as seen in Table 1, the OH concentration in the free stream, denoted hereafter as $[OH]_\infty$, ranged from 1.1 to 6.8×10^9 cm^{-3}. The self-reaction

$$2OH \xrightarrow{+M} H_2O_2 \quad \text{(R8)}$$

of OH was found to be unimportant within the ranges of $[OH]_\infty$ values and the flow residence time considered.

To ensure complete deliquescence of the NaCl particles, the relative humidity was raised to 85% for several minutes before lamp irradiation. From the onset of reaction, the relative humidity was kept at 70−80%. Because the efflorescence RH of NaCl is 44%, the particles were in the liquid state for all experiments.

CCSEM/EDX Single-Particle Analysis. Scanning electron microscopy (SEM) coupled with energy-dispersed X-ray (EDX) spectrometry was used to determine the elemental composition and loading density of NaCl particles. This instrument incorporated a FEI XL30 digital field emission gun environmental SEM. The microscope is equipped with an EDAX spectrometer (EDAX, Inc., model PV7761/54 ME) with a Si(Li) detector of an active area of 30 mm^2 and an ATW2 window, which allows X-ray detection from elements higher than beryllium ($Z > 4$). The system is equipped with *Genesis* hardware and software (EDAX, Inc.) for computer-controlled SEM/EDX particle analysis. Using this CCSEM/EDX setup, a matrix of fields of view was first defined over a sample area, which was then inspected automatically on a field-by-field basis. Particles are recognized by an increase in the detector signal above a threshold level. The program acquires an X-ray spectrum from each detected particle. Particle imaging[77] was made by acquiring the mixed signal of backscattered (BSE) and transmitted (TE) electrons. During the X-ray acquisition, the electron beam scans over the particle projection area. The X-ray spectra were acquired for 20 s, at a beam current of ~500 pA and an accelerating voltage of 20 kV. These conditions are sufficient to collect ~4000 photon counts per Na and Cl characteristic peaks. For quantification of the EDX results, the *Genesis* software utilizes a standardless microanalysis method which relates the measured X-ray intensities to elemental concentrations through theoretically calculated equivalent intensities of corresponding peaks. Specific details of the *Genesis*-enable microanalysis method can be found elsewhere.[80]

Experimental Protocol. The substrate-deposited NaCl particles at various surface densities were exposed to a controlled amount of OH in the reaction cell described above. A constant flow of $O_3/O_2/H_2O/N_2$ passed through the cell under UV radiation to provide a constant concentration of $[OH]_\infty$ in the mean free stream.

The change in the Cl-to-Na ratio ($[Cl/Na]_t^{EDX}$) in reacted particles was taken to reflect the chloride loss due to oxidation, i.e.

$$\frac{[Cl^-]_{d,t}}{[Cl^-]_{d,t=0}} = \frac{[Cl/Na]_t^{EDX}}{[Cl/Na]_{t=0}^{EDX}} \quad (1)$$

where the subscript d denotes the concentration in the NaCl droplet and t denotes the reaction time. Three series of experiments were conducted over a range of OH concentrations (1.1, 2.1, and 6.8×10^9 cm^{-3}). In each series of experiments, at least two reaction times were used. We also examined the reaction rates as a function of particle number density N_s on the substrate surface. The N_s value ranged from 1×10^4 to 5×10^7 particles cm^{-2}. A total of 91 samples were analyzed. Out of them, 15 samples with high particle density ($> 3 \times 10^6$ particles cm^{-2}) showed no statistically significant losses of chloride (where the mean $[Cl/Na]_t^{EDX}$ values were within 1 standard deviation of $[Cl/Na]_{t=0}^{EDX}$). In these samples, particles were too tightly packed on the substrate, which resulted in their reaction being too slow and generating significant compositional changes over the time period of individual experiments. Seventy-six samples with lower densities showed detectable losses of chloride. These samples are summarized in Table 1.

Additional experiments were conducted in order to ensure that the observed loss of chloride in the reacted particles is not due to oxidation by ozone or molecular oxygen. In these experiments, NaCl particle samples were exposed for 9 h to 2000 ppm of ozone in the same mixture of $O_3/O_2/H_2O/N_2$ gases but in the absence of UV radiation. Another exposure was conducted also for 9 h with UV radiation but without ozone. No changes in the Cl-to-Na ratios were detected in these experiments.

Results and Discussion

Apparent Pseudo First-Order And Intrinsic Second-Order Rate Constants. As seen in eq 1, CCSEM/EDX analysis

TABLE 1: Experimental Conditions and Summary of Pseudo First-Order Rate Constants[a]

exptl series	$N_s \times 10^{-4}$ (cm^{-2})	$[Cl/Na]_t^{EDX}/[Cl/Na]_{t=0}^{EDX}$	$k_I \times 10^6$ (s^{-1})	$N_s \times 10^{-4}$ (cm^{-2})	$[Cl/Na]_t^{EDX}/[Cl/Na]_{t=0}^{EDX}$	$k_I \times 10^6$ (s^{-1})
A1:						
		$t = 3$ h; $[Cl/Na]_{t=0}^{EDX} = 1.07 \pm 0.04$; $[OH]_\infty = 1.1 \times 10^9$ cm^{-3} ($O_3 = 1.9\%$; UV power = 100 W)				
	5 ± 5	0.87 ± 0.07	13 (+8/−7)	62 ± 19	0.92 ± 0.06	7.8 (+6.1/−5.8)
	9 ± 8	0.88 ± 0.06	12 (+7/−6)	68 ± 23	0.92 ± 0.05	7.4 (+5.3/−5.1)
	17 ± 10	0.90 ± 0.06	9.4 (+6.4/−6.0)	73 ± 30	0.94 ± 0.05	5.7 (+5.0/−4.8)
	19 ± 9	0.89 ± 0.05	11 (+6/−5)	95 ± 32	0.92 ± 0.05	7.4 (+5.0/−4.7)
	30 ± 18	0.93 ± 0.05	6.4 (+5.1/−4.9)	121 ± 32	0.95 ± 0.04	4.9 (+4.3/−4.1)
A2:						
		$t = 6$ h; $[Cl/Na]_{t=0}^{EDX} = 1.07 \pm 0.04$; $[OH]_\infty = 1.1 \times 10^9$ cm^{-3} ($O_3 = 1.9\%$; UV power = 100 W)				
	5 ± 2	0.62 ± 0.18	22 (+16/−12)	83 ± 43	0.91 ± 0.06	4.6 (+3.1/−2.9)
	13 ± 10	0.62 ± 0.18	22 (+16/−12)	88 ± 42	0.90 ± 0.06	5.0 (+3.2/−3.0)
	13 ± 9	0.71 ± 0.18	16 (+13/−10)	139 ± 69	0.92 ± 0.05	4.0 (+2.8/−2.7)
	21 ± 15	0.76 ± 0.16	13 (+11/−9)	220 ± 41	0.93 ± 0.06	3.5 (+3.2/−3.0)
	29 ± 15	0.72 ± 0.17	15 (+12/−10)	240 ± 44	0.90 ± 0.08	5.1 (+4.1/−3.7)
	41 ± 24	0.78 ± 0.17	11 (+11/−9)	241 ± 53	0.93 ± 0.05	3.3 (+2.6/−2.5)
	54 ± 28	0.82 ± 0.10	9.4 (+6.3/−5.6)	250 ± 50	0.93 ± 0.05	3.2 (+2.6/−2.5)
	81 ± 33	0.84 ± 0.09	8.0 (+5.5/−4.9)	303 ± 57	0.94 ± 0.04	2.8 (+2.2/−2.1)
B1:						
		$t = 1.5$ h; $[Cl/Na]_{t=0}^{EDX} = 1.07 \pm 0.04$; $[OH]_\infty = 2.1 \times 10^9$ cm^{-3} ($O_3 = 0.2\%$; UV power = 1000 W)				
	2 ± 1	0.72 ± 0.11	60 (+31/−27)	15 ± 10	0.80 ± 0.12	42 (+30/−26)
	1 ± 1	0.72 ± 0.19	62 (+58/−44)	23 ± 14	0.88 ± 0.06	24 (+13/−13)
	1 ± 1	0.71 ± 0.08	63 (+22/−20)	26 ± 14	0.92 ± 0.05	15 (+11/−10)
	2 ± 1	0.82 ± 0.07	36 (+17/−16)	35 ± 17	0.83 ± 0.11	35 (+26/−23)
	12 ± 8	0.85 ± 0.09	31 (+21/−19)	38 ± 15	0.89 ± 0.08	22 (+17/−16)
	13 ± 10	0.76 ± 0.09	51 (+23/−21)	40 ± 17	0.92 ± 0.06	16 (+13/−12)
B2:						
		$t = 3$ h; $[Cl/Na]_{t=0}^{EDX} = 1.07 \pm 0.04$; $[OH]_\infty = 2.1 \times 10^9$ cm^{-3} ($O_3 = 0.2\%$; UV power = 1000 W)				
	1 ± 1	0.58 ± 0.18	50 (+35/−25)	32 ± 15	0.90 ± 0.06	10 (+7/−6)
	5 ± 4	0.75 ± 0.15	27 (+21/−17)	46 ± 26	0.90 ± 0.05	10 (+5/−5)
	7 ± 4	0.71 ± 0.10	32 (+14/−13)	64 ± 28	0.93 ± 0.05	6.7 (+5.3/−5.0)
	25 ± 14	0.87 ± 0.06	13 (+7/−6)	66 ± 27	0.92 ± 0.06	7.7 (+6.0/−5.7)
	27 ± 20	0.91 ± 0.06	9.2 (+6.3/−5.9)			
B3:						
		$t = 4.5$ h; $[Cl/Na]_{t=0}^{EDX} = 1.07 \pm 0.04$; $[OH]_\infty = 2.1 \times 10^9$ cm^{-3} ($O_3 = 0.2\%$; UV power = 1000 W)				
	4 ± 3	0.60 ± 0.10	48 (+16/−14)	6 ± 5	0.71 ± 0.13	31 (+18/−15)
	5 ± 4	0.56 ± 0.26	54 (+59/−36)	68 ± 32	0.91 ± 0.06	8.4 (+6.2/−5.8)
C1:						
		$t = 0.5$ h; $[Cl/Na]_{t=0}^{EDX} = 1.06 \pm 0.05$; $[OH]_\infty = 6.8 \times 10^9$ cm^{-3} ($O_3 = 1.9\%$; UV power = 1000 W)				
	6 ± 3	0.81 ± 0.08	116 (+61/−55)	14 ± 10	0.89 ± 0.07	67 (+47/−43)
	7 ± 4	0.87 ± 0.07	77 (+46/−43)	15 ± 12	0.90 ± 0.07	56 (+42/−39)
	10 ± 5	0.85 ± 0.09	93 (+62/−56)	16 ± 9	0.90 ± 0.06	57 (+40/−38)
	17 ± 7	0.91 ± 0.06	50 (+40/−37)			
C2:						
		$t = 1$ h; $[Cl/Na]_{t=0}^{EDX} = 1.06 \pm 0.05$; $[OH]_\infty = 6.8 \times 10^9$ cm^{-3} ($O_3 = 1.9\%$; UV power = 1000 W)				
	6 ± 3	0.45 ± 0.10	220 (+68/−55)	15 ± 5	0.76 ± 0.07	78 (+25/−23)
	8 ± 5	0.48 ± 0.21	201 (+159/−101)	17 ± 12	0.86 ± 0.08	40 (+27/−24)
	9 ± 6	0.63 ± 0.15	127 (+77/−60)	18 ± 12	0.69 ± 0.15	103 (+69/−55)
	12 ± 6	0.62 ± 0.15	131 (+76/−59)	24 ± 14	0.68 ± 0.13	106 (+56/−47)

[a] Surface number density N_s (the uncertainty values are 1 standard deviation); the uncertainty values shown for $[Cl/Na]_t^{EDX}/[Cl/Na]_{t=0}^{EDX}$ represent 1 standard deviation, determined from the combined uncertainties of $[Cl/Na]_t^{EDX}$ and $[Cl/Na]_{t=0}^{EDX}$ values measured for a large number of particles; k_I apparent pseudo first-order rate constant of Cl^- disappearance, determined from eq 3 and the uncertainty values in the parentheses correspond to ± 1 standard deviation in $[Cl/Na]_t^{EDX}/[Cl/Na]_{t=0}^{EDX}$.

measures the overall Cl^- loss from the droplets, which can be expressed in the form of eq 2

$$-\frac{d[Cl^-]_d}{dt} = k_I[Cl^-]_d \qquad (2)$$

where $[Cl^-]_d$ is the molar concentration of Cl^- in the NaCl droplet. If the apparent pseudo first-order rate constant k_I is constant during reaction, its value may be obtained from

$$k_I = -\frac{1}{t}\ln\frac{[Cl^-]_{d,t}}{[Cl^-]_{d,0}} = -\frac{1}{t}\ln\frac{[Cl/Na]_t^{EDX}}{[Cl/Na]_{t=0}^{EDX}} \qquad (3)$$

Table 1 lists the experimentally observed $[Cl/Na]_t^{EDX}/[Cl/Na]_{t=0}^{EDX}$ and k_I values. The uncertainty values represent 1 standard deviation for $[Cl/Na]_t^{EDX}/[Cl/Na]_{t=0}^{EDX}$, obtained by statistical sampling of the normally distributed $[Cl/Na]_{t=0}^{EDX}$ and $[Cl/Na]_t^{EDX}$ data.

The pseudo first-order rate constant may be plotted in the form of $1/k_I$ as a function of N_s, as shown in Figure 3 for the three OH concentrations used in this study. The different data sets within each plot in Figure 3 represent different reaction times for a given concentration of gas-phase OH. While there is no consistent dependence on reaction time, the pseudo first-order rate constant does depend strongly on the particle loading on the substrate, N_s.

In the case of airborne particles, the experimentally measured chlorine loss can be related to various physical and chemical

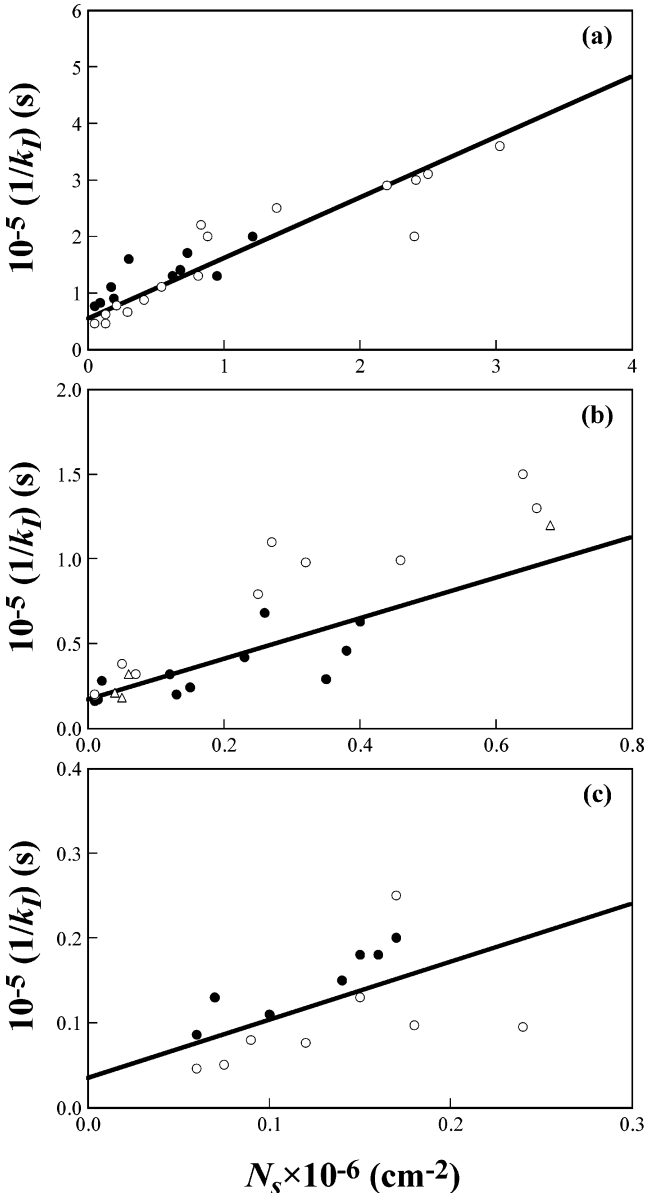

Figure 3. Experimental values (symbols) of $1/k_I^{exp}$ as a function of particle density on the substrate surface (N_s) and linear fits to data (lines) using eq 7: (a) ● and ○, experiments A_1 and A_2, respectively; (b) ●, ○, △, experiments B_1, B_2, and B_3, respectively; (c) ●, ○, experiments C_1 and C_2, respectively. See Table 1 for details.

processes occurring in the gas-particle system. These processes include the diffusion of gaseous OH to the particle surface, the kinetics of OH uptake, and the surface reactions. If the uptake of OH by the particles is fast, diffusion of OH to the surface can become rate-limiting. In this case, the concentration of OH at the particle surface will be smaller than that in the bulk gas phase, and the rate of oxidation of chloride ions in the particles is smaller than what would be the case without this diffusion limitation.

In the case of particles sequestered on a plane as in the present experiments, the changes in the OH concentration at the surface of the particles are also due to the competition for OH among adjacent droplets, which increases with increasing surface densities, N_s. It is this dependence on N_s that allows us to obtain the experimental reaction kinetics which resembles the airborne case by extrapolating the data to the $N_s \rightarrow 0$ limit.

The intrinsic, second-order rate constant k_{II} for reaction R3 is related to the pseudo first-order rate constant by

$$k_I = k_{II}[OH]_s \tag{4}$$

where $[OH]_s$ is the concentration of OH immediately above the droplet surface and, for reasons discussed already, may be lower than that in the free stream, i.e., at infinite distance from the particle surface, $[OH]_\infty$. Thus, while k_I depends on both the intrinsic reaction rate and the gas-phase diffusion rate, k_{II}, which reflects the fundamental reaction kinetics, does not depend on diffusion.

The data on the loss of chloride from the particles can be used to obtain k_I (eq 3) as a function of N_s. Previous studies show that the $OH-Cl^-$ reaction occurs at the interface.[67] However, the loss of Cl^- from the interface results in an equivalent depletion of Cl^- from the droplet, so that the measured chloride loss can be related to the reaction probability γ for the interface reaction (R3) in the following manner. First, to obtain k_{II} from the measured values of k_I (eq 4), the concentration of OH at the surface must be known. This is determined by a combined analysis of the concentration of OH in the free stream, its diffusion to the particle, and the reaction at the surface. In this work, gas-phase diffusion of OH to particles sequestered on the substrate has been approximated by a one-dimensional model of a stagnant gas film above the substrate surface (though locally the transport process is inherently multidimensional). In this approximation, the molar diffusion flux j_{OH} is equated with the removal rate of OH by the reacting particles as well as by the underlying substrate, i.e.

$$j_{OH} = -D_{OH}\frac{d[OH]}{dx} = N_s k_I [Cl^-]_d V_d + k_s[OH]_s \tag{5}$$

where D_{OH} is the gas-phase diffusion coefficient, x is the distance from the substrate, V_d is the NaCl droplet volume, and k_s is the rate constant for OH destruction by the substrate surface. Equation 5 may be integrated, and after applying appropriate boundary conditions, i.e., $[OH]_{x=L} = [OH]_\infty$ and $[OH]_{x=0} = [OH]_s$, we obtain (see Appendix A)

$$\frac{1}{k_I} = \frac{1}{[OH]_\infty}\left[\frac{(1+\delta k_s)}{k_{II}} + V_d[Cl^-]_{d,0}\delta e^{-k_I t}\cdot N_s\right] \tag{6}$$

Here, $\delta = L/D_{OH}$ and L is the characteristic diffusion length. Equation 6 gives a linear dependence of $1/k_I$ on N_s

$$\frac{1}{k_I} = \frac{1}{[OH]_\infty}(a + bN_s) \tag{7}$$

where $a = (1 + \delta k_s)/k_{II}$ and $b = V_d[Cl^-]_{d,0}\delta e^{-k_I t}$. It follows that $(1 + \delta k_s)/k_{II}$ may be determined from the intercept of a linear fit of the data plotted in Figure 3, provided that $[OH]_\infty$ is known and the parameter b is constant. In fact, b depends on $e^{-k_I t}$ and on the droplet volume V_d and δ, both of which may also change with time. For example, V_d may increase due to water uptake as the NaCl is converted to the mixture[68] of NaOH and $NaClO_x$, which are more hygroscopic. On the other hand, the characteristic diffusion length L, and hence δ, may decrease as the reaction proceeds and the chloride is consumed from the NaCl droplets. However, the data in Figure 3 do not exhibit a consistent trend with time, so that the net effect of changes in these three parameters must be small. Since $\delta k_s \geq 0$, the current

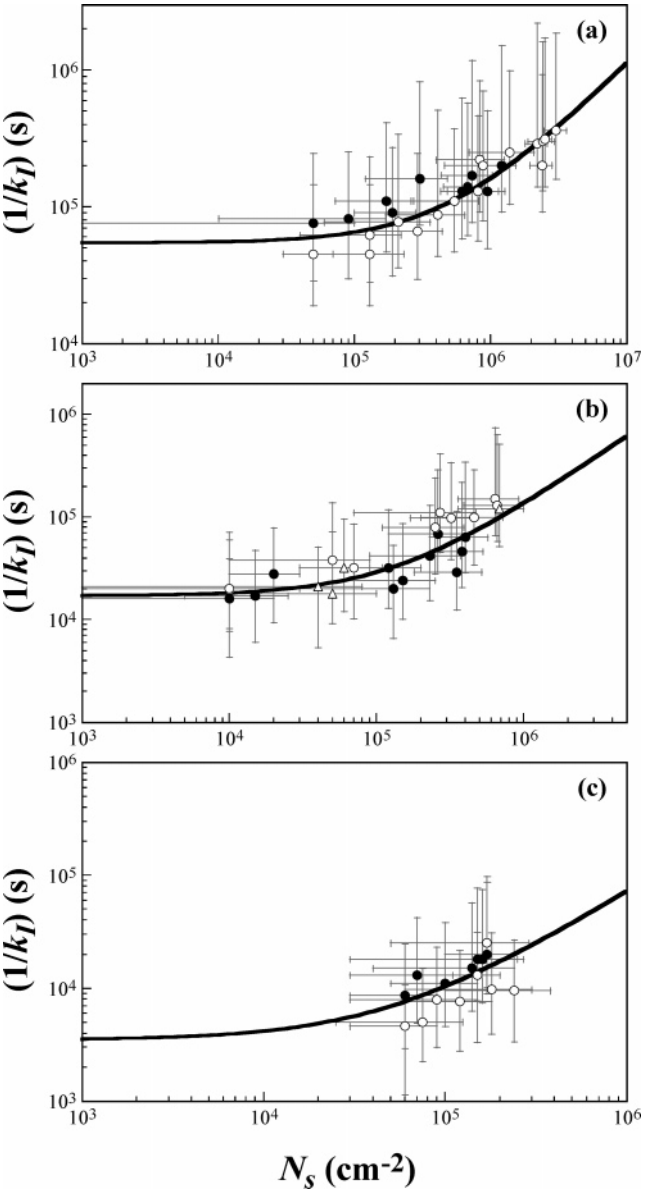

Figure 4. Experimental values (symbols) of $1/k_I^{exp}$ as a function of particle density on the substrate surface (N_s) and fits to data (dark lines) using eq 7: (a) ● and ○, experiments A_1 and A_2, respectively; (b) ●, ○, △, experiments B_1, B_2, and B_3, respectively; (c) ●, ○, experiments C_1 and C_2, respectively. See Table 1 for data details and corresponding uncertainty values.

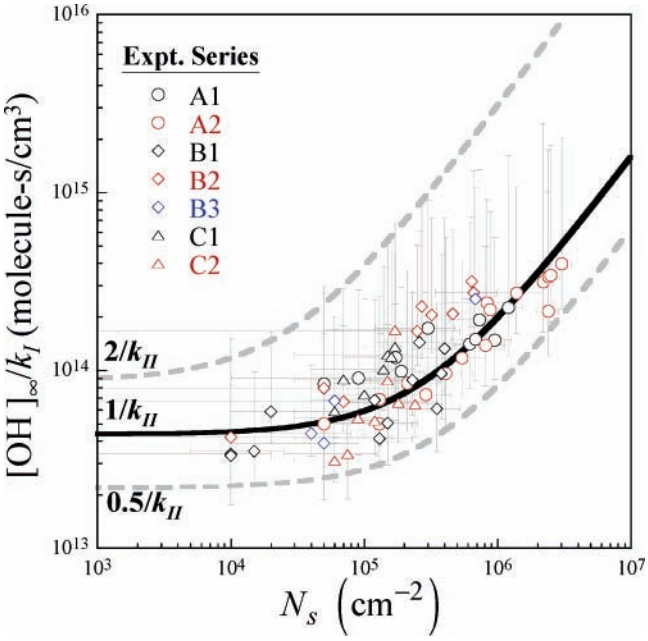

Figure 5. Experimental values (symbols) of $[OH]_\infty/k_I$ for all series of experiments as a function of particle density on the substrate surface (N_s). The solid line is the fit to data using eq 7; dashed lines represent the (×/÷ 2) uncertainty bounds for k_{II}, based on 1 standard deviation of the $[Cl/Na]_i^{EDX}$ values measured for a statistically significant number of droplets. See Table 1 for data details and corresponding uncertainty values.

experiment can only measure a lower limit for k_{II} (i.e., obtained with $k_s = 0$).

Linear extrapolation of the data in Figure 3 to $N_s = 0$ yielded $a = (6.0 \pm 2.6) \times 10^{13}$, $(3.6 \pm 1.2) \times 10^{13}$, and $(2.4 \pm 1.7) \times 10^{13}$ s for experimental series A, B, and C, respectively, where the uncertainty values represent 1 standard deviation as indicated in Table 1. Figure 4 shows the same data but plotted in log−log form, where the lines show the results of best linear fits. Lower limits to the corresponding values of k_{II} can be obtained from these values of a if it is assumed that $k_s = 0$, i.e., that there is no removal of OH by the substrate. Remerov and Bardwell[81] have developed a model for the uptake of OH on nonreactive surfaces where the OH is removed by reaction with a second OH on the surface. However, without knowledge of the energetics of interaction of OH with the TEM grid substrate material, we were not able to apply this model directly to calculate the loss of OH on the substrate surrounding the NaCl particles. However, while some loss of OH to the substrate is expected to occur, it cannot be very large, or a dependence of loss of chloride on N_s would not have been observed.

Figure 5 combines all three sets of data where the values of $[OH]_\infty/k_I$ are plotted as a function of particle density on the substrate surface (N_s). A fit to the combined data yields $k_{II} > 2.3 \times 10^{-14}$ cm^3 molecule^{-1} s^{-1} which, as discussed earlier, is a lower limit. The scatter of the data yielded an uncertainty factor of 2 (i.e., $1.15 \times 10^{-14} < k_{II} < 4.6 \times 10^{-14}$cm^3 molecule^{-1} s^{-1}), as demonstrated by the dashed lines in the same figure.

Reaction Probability. The net reaction probability (γ_{net}) is given by

$$\gamma_{net} = \frac{4k_I^*[Cl^-]_d V_d}{\bar{c}_{OH} S_d [OH]_\infty} = \frac{4k_{II}[Cl^-]_d V_d}{\bar{c}_{OH} S_d} \quad (8)$$

where V_d and S_d are the droplet volume and surface area, respectively, $\bar{c}_{OH}$ is the mean molecular speed of OH, and k_I^* is the apparent first-order rate constant in the $N_s \rightarrow 0$ limit. The reaction probability reported in this work is based on the intrinsic rate constant k_{II} averaged over the course of the reaction. Given that Cl^- decreases during the reaction, the value derived here for γ_{net} represents a lower limit to the reaction probability for OH with a deliquesced, unreacted particle.

The droplet volume V_d may be calculated, in principle, from the known dry particle diameter (selected by DMA before and confirmed by CCSEM analysis) and thermodynamic properties and hygroscopic growth data of NaCl particles.[53] Under our experimental conditions, $[Cl^-]_{d,0} = 5$ M and the ratio of mean droplet to dry particle diameters $\bar{D}_d/\bar{D}_p = 2$ at 80% RH, i.e., 0.9 μm dry NaCl particles become 1.8 μm deliquesced particles. At a somewhat lower RH value (i.e., the RH range of our

experiments is 70−80%), $[Cl^-]_{d,0} \times V_d$ in eq 8 should stay the same, but the surface area S_d would be smaller. Thus, the use of the droplet diameter at the higher end of the relative humidity results in a lower limit for γ_{net}.

Calculation of the surface area, S_d, available for reaction in the case of substrate-deposited particles requires knowledge of the particle morphology. Carbon thin film is substantially hydrophobic and effectively repels water even at supersaturation conditions.[77,82] Microscopic evidence indicates that a freshly deliquesced NaCl particle is well-approximated by a sphere tangent to the substrate.[74,82] In this case, S_d is approximately the surface area of a sphere $S_d = \pi \bar{D}_d^2$ (equal to 10 μm^2 here). However, SEM images taken after the reaction (see Figure 6) show a halo of residue around each vacuum-dried particle, indicating that the droplet wetted the substrate and spread to approximately twice its spherical wet diameter. We can assess the magnitude of this effect on our measurements by considering the reacted particle as a flattened sphere with volume equal to that of the spherical particle.

The surface area and volume of a flattened sphere can be calculated using the mensuration formulas

$$S_d = \pi D h \tag{9}$$

$$V_d = \frac{\pi h}{6}\left(h^2 + \frac{3d_{base}^{\ 2}}{4}\right) = \frac{\pi h^2}{3}\left(\frac{3D}{2} - h\right) \tag{10}$$

where h is the height of the segment and D is the diameter of a large sphere with the spherical cap of diameter d_{base}, which may be determined with the assumption that the volume of the spherical cap is equal to that of the sphere. A value for $d_{base} \approx 4$ μm can be estimated from the SEM images of the reacted NaCl particles (see Figure 6). For $\bar{D}_d = 1.82$ μm of the deliquesced NaCl particle at 80% RH, we calculate $h = 0.49$ μm and $D = 8.62$ μm for the spherical cap having an equivalent volume. On the basis of these parameters, eq 9 gives a surface area of $S_d \approx 13$ μm^2, about 30% higher than a perfect sphere with $\bar{D}_d = 1.82$ μm.

As shown in Table 2, reaction probabilities obtained using the k_{II} data are $\gamma_{net} \geq 0.13$ for spheres and 0.10 for flattened spheres. Again, the uncertainty factor is 2, derived from the standard deviation of $[Cl/Na]_t^{EDX}$ as discussed earlier.

Significance and Limitations of the Method. To the best of our knowledge, this is the first measurement of the net reaction probability for the reaction of gaseous OH radicals with deliquesced NaCl particles. Application to airborne particles is straightforward in that sea salt particles in air are sufficiently far apart that they do not exert an influence on adjacent particles. Under these conditions, there will still be a diffusion limitation for the case of reactions of micron-size particles with large reaction probabilities, because OH is removed more rapidly at the surface of individual particles than it can be replenished from the gas phase.[83] Because this applies both to the laboratory experiments as well as to airborne particles, our lower limit of ~0.1 for the initial, net reaction probability should still be applicable to ~2 μm deliquesced sea salt particles found in the marine boundary layer.

Several assumptions made in the data analysis deserve further discussion. These are as follows: (a) The substrate is unreactive, i.e., the OH consumption by the substrate does not substantially affect its local concentration ($\delta k_s \ll 1$ in eq 6); and (b) the extent of OH reaction with the deliquesced NaCl droplets can be obtained directly from EDX measurements of the vacuum-dried particles. In the first case, if some of the OH is removed by the substrate, values of k_I and the reaction probability γ_{net} would be underestimated. However, as discussed earlier, the data show that loss of OH to the NaCl particles is at least competitive with removal by the substrate, and we report the value of γ_{net} as a lower limit. The potential competition between reaction of OH with the substrate and with the particles of interest does imply that the presented method will be most useful for cases where the particles are highly reactive.

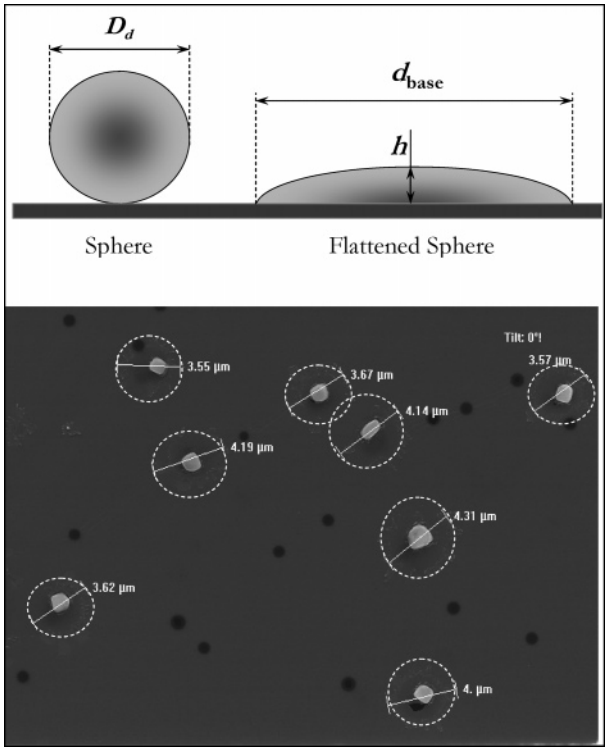

Figure 6. Upper panel: Assumed morphologies of the deliquesced NaCl droplets on a substrate. The sphere represents a freshly deliquesced NaCl particle, while the flattened sphere represents the particle after wetting the substrate. Its volume is approximated by that of a spherical cap of a large sphere of diameter D (not shown). Lower panel: SEM image of the NaCl particles after reaction and being dried in the vacuum chamber of the microscope during analysis. The observed halos suggest flattened spheres for the shapes of NaCl particles during the reaction.

The second assumption relies on the loss of chlorine from the particles to the gas phase being irreversible. EDX measurements cannot distinguish the chemical state of chlorine in particles. Some of the Cl_2 produced by the OH + $NaCl_{aq}$ reaction can be taken up into the particle as it becomes more basic and hydrolyze to form OCl^- which upon drying disproportionates to leave a combination of $NaClO_x$ species in the dry particles.[68] This would offset some of the initial chloride ion depletion and again lead to an underestimation of the reaction probability.

There are no previous direct measurements of the probability of reaction at the surface with which to compare the present results. The view of surface reactions such as that of gaseous OH with $NaCl_{aq}$ is that they occur in competition with mass accommodation,[59,84,85] that is, an incoming OH collides with the surface and is taken up into the bulk (mass accommodation), undergoes reaction at the surface, or scatters into the gas phase. Experimental measurements[86] of mass accommodation of OH on pure water placed a lower limit for the mass accommodation coefficient at 275 K of 0.0035, while a more recent study reported a lower limit of 0.01.[87] In those experiments, authors concerned that Henry's law surface saturation occurred on the

TABLE 2: Summary of Kinetic Data Measured for the $OH_g + NaCl_{aq}$ Reaction

exptl series	$[OH] \times 10^{-9}$ (molecule cm^{-3})	fitted parameters		$k_{II} \times 10^{14}$ [a] (cm^3 molecule^{-1} s^{-1})	γ_{net} [a,b]	
		$a \times 10^{-13}$ (s)	$b \times 10^{-8}$ (s/cm^2)		1.82 μm sphere	$d_{base} = 4$ μm flattened sphere
A	1.1	6.0 ± 2.6	1.2	1.8 ($\times/\div$ 1.8)	0.10 ($\times/\div$ 1.8)	0.08 ($\times/\div$ 1.8)
B	2.1	3.6 ± 1.2	2.5	3.0 ($\times/\div$ 1.5)	0.17 ($\times/\div$ 1.5)	0.13 ($\times/\div$ 1.5)
C[c]	6.8	2.4 ± 1.7	4.7	4.6 ($\times/\div$ 2.3)	0.25 ($\times/\div$ 2.3)	0.19 ($\times/\div$ 2.3)
fit to A and B[d]		6.0 ($\times/\div$ 1.8)	1.2	1.8 ($\times/\div$ 1.8)	0.10 ($\times/\div$ 1.8)	0.08 ($\times/\div$ 1.8)
fit to all data[d,e]		4.4 ($\times/\div$ 2)	1.6	2.3 ($\times/\div$ 2)	0.13 ($\times/\div$ 2)	0.10 ($\times/\div$ 2)

[a] Lower limit, calculated by assuming $k_s = 0$ (see text). [b] Calculated using eq 8 and $[Cl^-]_0 = 5$ M. [c] Because of the small number of samples and narrow range of N_s values employed, this set of data is of limited accuracy. [d] Excluding series C from the overall fit yields k_{II} and γ_{net} values well within the respective uncertainties of those from fit to all data. [e] Fits to data are shown in Figure 5. The uncertainty bounds are taken as a factor of 2, as seen by the dotted lines bracketing the data.

time scale of their respective experiments,[86,87] which is why the latter experiment,[87] with a shorter measurement time scale, reports a larger lower limit value. Molecular dynamics simulations[88,89] suggest it could be as large as 0.83, although such MD predictions tend to be higher than experimental measurements of reaction probability. For the OH reaction with chloride at the interface, computer kinetics modeling[73,85] of aerosol chamber studies of reaction R3 gave good fits to the experimentally measured production of Cl_2 using an overall reaction probability of ~0.2 for small particles (diameter around 200 nm) where the diffusion limitation is not important. There were a number of variables in the model for which data were not available, so that the net reaction probability was not uniquely defined by the experiments. However, with this caveat in mind, the lower limit for the overall reaction probability of ~0.1 obtained here is consistent with the value of 0.2 used in that that modeling study.

Conclusions

This study presents a new method for measuring net reaction probabilities for the reactions of gases with liquids or solids. The approach is expected to be applicable to a variety of reactions of interest not only for the atmospheric research community but also for the surface science and catalysis communities. The main requirements are that the substrate reactivity is small compared to that of the deposited particles and that a component of the particles that can be measured quantitatively change in response to the reaction. Application of this novel approach to the reaction of gaseous OH with deliquesced NaCl particles gives a lower limit to the reaction probability of $\gamma_{net} \geq 0.1$ with an uncertainty of a factor of 2.

Acknowledgment. The PNNL and the USC research groups acknowledge support provided by Tropospheric Chemistry and Radiation Sciences programs at the National Aeronautics and Space Administration (grants NNG06GE89G and NNG06GI51G). The UCI research group acknowledges support provided by the National Science Foundation through an Environmental Molecular Sciences Institute (grants CHE-0209719 and CHE-0431312). The experimental part of this work was performed in the William R. Wiley Environmental Molecular Sciences Laboratory, a national scientific user facility sponsored by the Department of Energy's Office of Biological and Environmental Research and located at Pacific Northwest National Laboratory (PNNL). PNNL is operated by the U. S. Department of Energy by Battelle Memorial Institute under contract no. DE-AC06-76RL0 1830.

Appendix A

The molar diffusion flux j_{OH} is equated to the removal rate of OH by the reacting particles and by the underlying substrate, i.e., eq 5 in the main text

$$j_{OH} = D_{OH}\frac{d[OH]}{dx} = N_s k_I [Cl^-]_d V_d + k_s [OH]_s \quad \text{(A1)}$$

Integrating eq A1, we obtain

$$D_{OH}[OH]_x = (N_s k_I [Cl^-]_d V_d + k_s [OH]_s)x + c \quad \text{(A2)}$$

Applying the boundary condition that $[OH]_{x=L} = [OH]_\infty$, i.e., the concentration of OH radicals at distance L from the substrate is equal to that in the free stream, we have

$$c = D_{OH}[OH]_\infty - (N_s k_I [Cl^-]_d V_d + k_s [OH]_s)L \quad \text{(A3)}$$

Combining eqs A2 and A3, we obtain the following equation

$$D_{OH}([OH]_x - [OH]_\infty) = (N_s k_I [Cl^-]_d V_d + k_s [OH]_s)(x - L) \quad \text{(A4)}$$

For $x = 0$, $[OH]_{x=0} = [OH]_s$. Combining eq A4 with $k_I = k_{II}$-$[OH]_s$ and $[Cl^-]_d = [Cl^-]_{d,0}e^{-k_I t}$, letting $\delta = L/D_{OH}$, and rearranging the resulted derivation, we obtain eq 6 of the main text

$$\frac{1}{k_I} = \frac{1}{[OH]_\infty}\left[\frac{(1 + \delta k_s)}{k_{II}} + V_d [Cl^-]_{d,0}\delta e^{-k_I t}\cdot N_s\right] \quad \text{(A5)}$$

References and Notes

(1) Robbins, R. C.; Cadle, R. D.; Eckhardt, D. L. *J. Meteorol.* **1959**, *16*, 53.
(2) Cadle, R. D.; Robbins, R. C. *Discuss. Faraday Soc.* **1960**, *30*, 155.
(3) Schroeder, W. H.; Urone, P. *Environ. Sci. Technol.* **1974**, *8*, 756.
(4) Cicerone, R. J. *Rev. Geophys. Space Phys.* **1981**, *19*, 123.
(5) Finlayson-Pitts, B. J. *Nature (London)* **1983**, *306*, 676.
(6) *Simulation of Atmospheric Photochemistry in the Presence of Solid Airborne Aerosols*; Zetzsch, C., Ed.; VCH Publishers: Weinheim, 1987; Vol. 104, pp 187.
(7) Zetzsch, C.; Pfahler, G.; Behnke, W. *J. Aerosol Sci.* **1988**, *19*, 1203.
(8) Behnke, W.; Zetzsch, C. *J. Aerosol Sci.* **1989**, *20*, 1167.
(9) *Smog Chamber Investigations of the Influence of NaCl Aerosol on the Concentration of O_3 in a Photosmog System*; Behnke, W., Zetzsch, C., Eds.; Deepak Publishing: New York, 1989; p 519.
(10) Behnke, W.; Zetzsch, C. *J. Aerosol Sci.* **1990**, *21*, S229.
(11) Behnke, W.; Kruger, H.-U.; Scheer, V.; Zetzsch, C. *J. Aerosol Sci.* **1991**, *22*, S609.
(12) Zetzsch, C.; Behnke, W. *Ber. Bunsen-Ges. Phys. Chem.* **1992**, *96*, 488.
(13) *Heterogeneous Reactions of Chlorine Compounds*; Zetzsch, C., Behnke, W., Eds.; Springer-Verlag: Berlin, 1993; Vol. 17, p 291.
(14) Behnke, W.; Scheer, V.; Zetzsch, C. *J. Aerosol Sci.* **1993**, *24*, 5115.

(15) Behnke, W.; Scheer, V.; Zetzsch, C. *J. Aerosol Sci.* **1994**, *S25*, 277.
(16) Behnke, W.; Scheer, V.; Zetzsch, C. Production of a Photolytic Precursor of Atomic Cl from Aerosols and Cl^- in the Presence of O_3. In *Naturally-Produced Organohalogens*; Grimwall, A., Leer, E. W. B. d., Eds.; Academic Publishers: Dordrecht, 1995; p 375.
(17) Leu, M.-T.; Timonen, R. S.; Keyser, L. F. *J. Phys. Chem. A* **1997**, *101*, 278.
(18) Leu, M.-T.; Timonen, R. S.; Keyser, L. F.; Yung, Y. L. *J. Phys. Chem.* **1995**, *99*, 13203.
(19) Laux, J. M.; Hemminger, J. C.; Finlayson-Pitts, B. J. *Geophys. Res. Lett.* **1994**, *21*, 1623.
(20) Fenter, F. F.; Caloz, F.; Rossi, M. J. *J. Phys. Chem.* **1994**, *98*, 9801.
(21) Allen, H. C.; Laux, J. M.; Vogt, R.; Finlayson-Pitts, B. J.; Hemminger, J. C. *J. Phys. Chem.* **1996**, *100*, 6371.
(22) Fenter, F. F.; Caloz, F.; Rossi, M. J. *J. Phys. Chem.* **1996**, *100*, 1008.
(23) Fenter, F. F.; Caloz, F.; Rossi, M. J. *Rev. Sci. Instrum.* **1997**, *68*, 3180.
(24) Laux, J. M.; Fister, T. F.; Finlayson-Pitts, B. J.; Hemminger, J. C. *J. Phys. Chem.* **1996**, *100*, 19891.
(25) Davies, J. A.; Cox, R. A. *J. Phys. Chem. A* **1998**, *102*, 7631.
(26) Ten Brink, H. M. *J. Aerosol Sci.* **1998**, *29*, 57.
(27) Abbatt, J. P. D.; Waschewsky, G. C. G. *J. Phys. Chem. A* **1998**, *102*, 3719.
(28) Behnke, W.; Elend, M.; Kruger, U.; Zetzsch, C. *J. Atmos. Chem.* **1999**, *34*, 87.
(29) Koch, T. G.; van den Bergh, H.; Rossi, M. J. *Phys. Chem. Chem. Phys.* **1999**, *1*, 2687.
(30) Finlayson-Pitts, B. J.; Johnson, S. N. *Atmos. Environ.* **1988**, *22*, 1107.
(31) Finlayson-Pitts, B. J.; Livingston, F. E.; Berko, H. N. *Nature (London)* **1990**, *343*, 622.
(32) Ravishankara, A. R. *Science* **1997**, *276*, 1058.
(33) Andreae, M. O.; Crutzen, P. J. *Science* **1997**, *276*, 1052.
(34) Ghosal, S.; Hemminger, J. C. *J. Phys. Chem. A* **1999**, *103*, 4777.
(35) Guimbaud, C.; Arens, F.; Gutzwiller, L.; Gaggeler, H. W.; Ammann, M. *Atmos. Chem. Phys.* **2002**, *2*, 249.
(36) Ghosal, S.; Hemminger, J. C. *J. Phys. Chem. B* **2003**, *108*, 14102.
(37) Rossi, M. J. *Chem. Rev.* **2003**, *103*, 4823.
(38) Finlayson-Pitts, B. J. *Chem. Rev.* **2003**, *103*, 4801.
(39) Thornton, J. A.; Abbatt, J. P. D. *J. Phys. Chem. A* **2005**, *109*, 10004.
(40) Finlayson-Pitts, B. J. *Chem. Rev.* **2003**, *103*, 4801.
(41) Rossi, M. J. *Chem. Rev.* **2003**, *103*, 4823.
(42) Keene, W. C.; Jacob, D. J.; Fan, S. M. *Atmos. Environ.* **1996**, *30*, R1.
(43) Keene, W. C.; Khalil, M. A. K.; Erickson, D. J.; McCulloch, A.; Graedel, T. E.; Lobert, J. M.; Aucott, M. L.; Gong, S. L.; Harper, D. B.; Kleiman, G.; Midgley, P.; Moore, R. M.; Seuzaret, C.; Sturges, W. T.; Benkovitz, C. M.; Koropalov, V.; Barrie, L. A.; Li, Y. F. *J. Geophys. Res., [Atmos.]* **1999**, *104*, 8429.
(44) Khalil, M. A. K.; Moore, R. M.; Harper, D. B.; Lobert, J. M.; Erickson, D. J.; Koropalov, V.; Sturges, W. T.; Keene, W. C. *J. Geophys. Res., [Atmos.]* **1999**, *104*, 8333.
(45) Erickson, D. J.; Seuzaret, C.; Keene, W. C.; Gong, S. L. *J. Geophys. Res., [Atmos.]* **1999**, *104*, 8347.
(46) Finlayson-Pitts, B. J.; Hemminger, J. C. *J. Phys. Chem. A* **2000**, *104*, 11463.
(47) Sander, R.; Keene, W. C.; Pszenny, A. A. P.; Arimoto, R.; Ayers, G. P.; Baboukas, E.; Cainey, J. M.; Crutzen, P. J.; Duce, R. A.; Honninger, G.; Huebert, B. J.; Maenhaut, W.; Mihalopoulos, N.; Turekian, V. C.; Van Dingenen, R. *Atmos. Chem. Phys.* **2003**, *3*, 1301.
(48) Knipping, E. M.; Dabdub, D. *Environ. Sci. Technol.* **2003**, *37*, 275.
(49) Blanchard, D. C.; Woodcock, A. H. *Ann. N. Y. Acad. Sci.* **1980**, *338*, 330.
(50) O'Dowd, C. D.; Smith, M. H. *J. Geophys. Res.* **1993**, *98*, 1137.
(51) Hoppel, W. A.; Frick, G. M.; Fitzgerald, J. W. *J. Geophys. Res., [Atmos.]* **2002**, *107*, 4382.
(52) Gong, S. L. *Global Biogeochem. Cycles* **2003**, *17*, article no. 1097.
(53) Tang, I. N.; Tridico, A. C.; Fung, K. H. *J. Geophys. Res., [Atmos.]* **1997**, *102*, 23269.
(54) Harvie, C. E.; Weare, J. H.; Hardie, L. A.; Eugster, H. P. *Science* **1980**, *208*, 498.
(55) Laskin, A.; Cowin, J. P.; Iedema, M. J.; Gaspar, D. J. Off-line Analysis of Aerosols: Exploring Heterogeneous Chemistry of Individual Atmospheric Particles. In *Combustion and Pollution: Environmental Impact*; Roy, G. D., Frolov, S. M., Starik, A. M., Eds.; Torus Press: Moscow, 2005; p 229.
(56) Hanson, D. R.; Ravishankara, A. R. *J. Phys. Chem.* **1994**, *98*, 5728.
(57) George, C.; Behnke, W.; Scheer, V.; Zetzsch, C.; Magi, L.; Ponche, J. L.; Mirabel, P. *Geophys. Res. Lett.* **1995**, *22*, 1505.
(58) Katrib, Y.; Deiber, G.; Schweitzer, F.; Mirabel, P.; George, C. *J. Aerosol Sci.* **2001**, *32*, 893.
(59) Hu, J. H.; Shi, Q.; Davidovits, P.; Worsnop, D. R.; Zahniser, M. S.; Kolb, C. E. *J. Phys. Chem.* **1995**, *99*, 8768.
(60) Abelson, P. H. *Science* **1997**, *277*, 15.
(61) Oum, K. W.; Lakin, M. J.; Finlayson-Pitts, B. J. *Geophys. Res. Lett.* **1998**, *25*, 3923.
(62) Hunt, S. W.; Roeselova, M.; Wang, W.; Wingen, L. M.; Knipping, E. M.; Tobias, D. J.; Dabdub, D.; Finlayson-Pitts, B. J. *J. Phys. Chem. A* **2004**, *108*, 11559.
(63) Jungwirth, P.; Tobias, D. J. *J. Phys. Chem. B* **2000**, *104*, 7702.
(64) Jungwirth, P.; Tobias, D. J. *J. Phys. Chem. B* **2001**, *105*, 10468.
(65) Jungwirth, P.; Tobias, D. J. *J. Phys. Chem. B* **2002**, *106*, 6361.
(66) Jungwirth, P.; Tobias, D. J. *J. Phys. Chem. A* **2002**, *106*, 379.
(67) Knipping, E. M.; Lakin, M. J.; Foster, K. L.; Jungwirth, P.; Tobias, D. J.; Gerber, R. B.; Dabdub, D.; Finlayson-Pitts, B. J. *Science* **2000**, *288*, 301.
(68) Laskin, A.; Gaspar, D. J.; Wang, W.; Hunt, S. W.; Cowin, J. P.; Colson, S. D.; Finlayson-Pitts, B. J. *Science* **2003**, *301*, 340.
(69) Oum, K. W.; Lakin, M. J.; DeHaan, D. O.; Brauers, T.; Finlayson-Pitts, B. J. *Science* **1998**, *279*, 74.
(70) Roeselova, M.; Jungwirth, P.; Tobias, D. J.; Gerber, R. B. *J. Phys. Chem. B* **2003**, *107*, 12690.
(71) Roeselova, M.; Vieceli, J.; Dang, L. X.; Garrett, B. C.; Tobias, D. J. *J. Am. Chem. Soc.* **2004**, *126*, 16308.
(72) Vieceli, J.; Roeselova, M.; Potter, N.; Dang, L. X.; Garrett, B. C.; Tobias, D. J. *J. Phys. Chem. B* **2005**, *109*, 15876.
(73) Knipping, E. M.; Dabdub, D. *J. Geophys. Res.* **2002**, *107*, 4360.
(74) Krueger, B. J.; Grassian, V. H.; Iedema, M. J.; Cowin, J. P.; Laskin, A. *Anal. Chem.* **2003**, *75*, 5170.
(75) Krueger, B. J.; Grassian, V. H.; Laskin, A.; Cowin, J. P. *Geophys. Res. Lett.* **2003**, *30* (3), 1148.
(76) Laskin, A.; Wietsma, T. W.; Grassian, V. H.; Krueger, B. J. *J. Geophys. Res., [Atmos.]* **2005**, *110*, D10208.
(77) Laskin, A.; Cowin, J. P.; Iedema, M. J. *J. Electron Spectrosc. Relat. Phenom.* **2006**, *150*, 260.
(78) Laskin, A.; Iedema, M. J.; Cowin, J. P. *Aerosol Sci. Technol.* **2003**, *37*, 246.
(79) Braun, W.; Herron, J. T.; Kahaner, D. K. *Int. J. Chem. Kinet.* **1988**, *20*, 51.
(80) Hua, Y. N. *J. Trace Microprobe Technol.* **2003**, *21*, 25.
(81) Remorov, R. G.; Bardwell, M. W. *J. Phys. Chem. B* **2005**, *109*, 20036.
(82) Ebert, M.; Inerle-Hof, M.; Weinbruch, S. *Atmos. Environ.* **2002**, *36*, 5909.
(83) Sander, R. *Rev. Geophys.* **1999**, *20*, 1.
(84) Hanson, D. R. *J. Phys. Chem.* **1997**, *101*, 4998.
(85) Thomas, J. L.; Jimenez-Aranda, A.; Finlayson-Pitts, B. J.; Dabdub, D. *J. Phys. Chem. A* **2006**, *110*, 1859.
(86) Hanson, D. R.; Burkholder, J. B.; Howard, C. J.; Ravishankara, A. R. *J. Phys. Chem.* **1992**, *96*, 4979.
(87) Takami, A.; Kato, S.; Shomono, A.; Koda, S. *Chem. Phys.* **1998**, *213*, 215.
(88) Roeselova, M.; Vieceli, J.; Dang, L. X.; Garrett, B. C.; Tobias, D. J. *J. Am. Chem. Soc.* **2004**, *126*, 16308.
(89) Vieceli, J.; Roeselova, M.; Potter, N.; Dang, L. X.; Garrett, B. C.; Tobias, D. J. *J. Phys. Chem. B* **2005**, *109*, 15876.